FEBS Letters 583 (2009) 1481–1488

journal homepage: www.FEBSLetters.org

Selective block of tunneling nanotube (TNT) formation inhibits intercellular organelle transfer between PC12 cells

Nickolay V. Bukoreshtliev [1], Xiang Wang [1], Erlend Hodneland [1], Steffen Gurke, João F.V. Barroso, Hans-Hermann Gerdes *

Department of Biomedicine, University of Bergen, Jonas Lies vei 91, 5009 Bergen, Hordaland, Norway

ARTICLE INFO

Article history:
Received 5 November 2008
Revised 16 March 2009
Accepted 28 March 2009
Available online 2 April 2009

Edited by Michael R. Bubb

Keywords:
Tunneling nanotube
Cytochalasin B
Intercellular organelle transfer
Filopodium

ABSTRACT

Organelle exchange between cells via tunneling nanotubes (TNTs) is a recently described form of intercellular communication. Here, we show that the selective elimination of filopodia from PC12 cells by 350 nM cytochalasin B (CytoB) blocks TNT formation but has only a weak effect on the stability of existing TNTs. Under these conditions the intercellular organelle transfer was strongly reduced, whereas endocytosis and phagocytosis were not affected. Furthermore, the transfer of organelles significantly correlated with the presence of a TNT-bridge. Thus, our data support that in PC12 cells filopodia-like protrusions are the principal precursors of TNTs and CytoB provides a valuable tool to selectively interfere with TNT-mediated cell-to-cell communication.

1. Introduction

Intercellular communication plays a central role in the physiology of multi-cellular organisms, and the exchange of molecular information is achieved by a variety of cellular mechanisms. Recently, a new principle of cell-to-cell communication based on the de novo formation of thin membrane channels between mammalian cells was documented [1]. These channels, referred to as tunneling nanotubes (TNTs), were shown to permit the direct intercellular transfer of endosome-related organelles and other cellular components [1]. Subsequently, TNT-like nanotubes were found to connect other cell types [2–4] and the transfer of mitochondria [5,6], plasma membrane components [1,7,8], calcium ions [8] as well as viral proteins [9,10] along TNT-like bridges was demonstrated. From these studies and the recent demonstration that TNT-connectivity exists in vivo between immune cells of the corneal stroma [11], it emerges that TNT-mediated communication has the potential to play an important role in many physiological processes of multi-cellular organisms.

TNT-like structures appear to form by two different mechanisms that may vary with cell type: by the directed outgrowth of a filopodium-like protrusion toward a neighboring cell or by dislodgement of attached cells after a certain required interaction time [3,4]. In contrast to filopodia, TNTs between cultured cells have no contact to the substratum but hover freely in the intercellular space. Filopodia along with lamellipodia are F-actin-based protrusive structures attached to the substratum of cultured cells with migratory and exploratory functions [12]. Filopodia have a rodlike shape and are filled with bundles of parallel actin filaments, whereas lamellipodia are flat protrusions with a meshwork of actin filaments. In contrast to lamellipodia, filopodia possess a so-called tip complex consisting of different anti-capping proteins and F-actin nucleators [13–15]. Interestingly, treatment with cytochalasin B/D in the nanomolar range has been an elegant way to specifically block filopodia formation in neuronal cell types [16,17]. The exact mode of action is not known, but it is presumed that at low concentrations cytochalasin B/D specifically compete with Ena/VASP proteins at the filopodial tip and thus, block the addition of actin monomers [16,17].

In this study, we investigated the effects of nanomolar concentrations of cytochalasin B (CytoB) on TNT formation and stability as well as on organelle exchange in PC12 cell cultures.

Abbreviations: TNT, tunneling nanotube; WGA488, Alexa Fluor® 488 wheat germ agglutinin; WGA633, Alexa Fluor® 633 wheat germ agglutinin; CTB, CellTracker™ Blue CMAC; CTG, CellTracker™ Green CMFDA; DiD, Vybrant® DiD cell-labeling solution; DiI, Vybrant® DiI cell-labeling solution; CytoB, cytochalasin B; DMSO, dimethylsulfoxide

* Corresponding author. Fax: +47 55586360.
E-mail address: hans-hermann.gerdes@biomed.uib.no (H.-H. Gerdes).
[1] These authors contributed equally to this work.

0014-5793/$36.00 © 2009 Federation of European Biochemical Societies. Published by Elsevier B.V. All rights reserved.
doi:10.1016/j.febslet.2009.03.065

2. Materials and methods

2.1. Reagents and cell culture

Alexa Fluor® 488 wheat germ agglutinin (WGA488), Alexa Fluor® 633 wheat germ agglutinin (WGA633), CellTracker™ Blue CMAC (CTB), CellTracker™ Green CMFDA (CTG), Vybrant® DiI cell-labeling solution (DiI) and Vybrant® DiD cell-labeling solution (DiD) were purchased from Molecular Probes (Invitrogen Detection Technologies, Carlsbad, CA, USA). CytoB was obtained from Sigma Aldrich (Sigma–Aldrich Corp., St. Louis, MO, USA). For all experiments, singularized PC12 cells (rat pheochromocytoma cells, clone 251, [18]) were plated at a density of 6×10^4 cells/cm^2 and cultured as described [1].

2.2. Imaging and FACS analysis

Confocal and wide-field microscopy were performed with a Leica TCS SP5 (Leica Microsystems GmbH, Wetzlar, Germany) and a Zeiss Axiovert 200M (Carl Zeiss, Jena, Germany) or an Olympus IX70 microscope (Olympus Optical Co., Europe GmbH, Hamburg, Germany), respectively, as described [19]. Flow cytometry analysis of organelle transfer was performed on a FACSCalibur™ flow cytometer (Becton–Dickinson, Mountain View, CA, USA) as described [19].

2.3. Analysis of organelle transfer

For quantitative analyses of TNT structures and intercellular organelle transfer, cocultures of CTB or CTG stained cells (acceptor population) and DiD stained cells (donor population) were plated at a ratio of 1:1. Notably, the DiD staining was performed 1 day before the start of the coculture. One hour after plating, the medium was removed to eliminate cell debris, and new medium containing 350 nM CytoB [1:1000 dilution from a 350 μM stock in dimethylsulfoxide (DMSO)] was added. The control cells were cultured without DMSO since additional experiments indicated that a 1:1000 dilution of DMSO had no effect on TNT number or organelle transfer (data not shown). Analysis of organelle transfer was performed at 2 and 24 h after cell plating. For microscopy analysis, WGA488 was added to the cells to permit cell segmentation and TNT detection (see Section 2.6). Image stacks covering the whole cellular volume were acquired by wide-field microscopy for the CTB, DiD and WGA488 channels using excitation wavelength of 400 nm, 633 nm and 488 nm, respectively. For FACS analysis, DiD-labeled donor cells and CTG-labeled acceptor cells were analyzed at 633 nm and 488 nm excitation wavelength, respectively.

2.4. Analysis of phagocytosis

Cell debris was generated by mechanical lysis of DiI-stained PC12 cells using a custom-made CellCracker. Then, a post-nuclear supernatant was prepared by centrifugation at 3000×*g* for 10 min. The supernatant was split into two equal portions, one was supplemented with 350 nM CytoB, and both portions were added to plated cells, respectively. As a control for the analysis algorithm, cells without added cell debris were incubated in the absence of CytoB in parallel. After 2 h of incubation, the different cell populations were washed, further incubated in growth medium in the absence or presence of CytoB and imaged 24 h later. Directly before the start of imaging, the growth medium was replaced by Tyrode's solution (2 mM $CaCl_2$, 2.5 mM KCl, 119 mM NaCl, 2 mM MgCb, 30 mM glucose, 25 mM HEPES, pH 7.4, 2 mM bromphenol blue) [20]. Notably, bromphenol blue quenches extracellular fluorescence signals and thus guarantees that only internalized signals are quantified. 3D image stacks for DiI fluorescence were acquired at 555 nm excitation wavelength using wide-field microscopy. Cell segmentation was performed on the same channel using the watershed method since the cells appeared as dark regions surrounded by brighter extracellular space (Fig. 4A). Phagocytosed cell debris was detected using adaptive thresholding.

2.5. Analysis of fluid-phase endocytosis

WGA633 was added to plated cells and incubated for 30 min at 37 °C in the presence or absence (control) of 350 nM CytoB, or at 0.7 °C in the absence of 350 nM CytoB. Subsequently, WGA488 was added and stacks of 20 focal planes spanning the whole cellular volume were recorded by wide-field microscopy at 488 nm and 633 nm excitation wavelength. The data were processed by 3D automated image segmentation using the WGA488 channel (see Section 2.6). The rate of endocytosis was determined by a quantitative analysis of the WGA633 signal within the cell regions. Signals were calculated by subtracting the mean signal intensity inside the cells from the mean signal intensity outside the cells, both applied to the WGA633.

2.6. Quantitative image processing

3D image stacks of WGA488-stained cells acquired by wide-field fluorescence microscopy were used for cell segmentation by applying automated marker construction [21] and the watershed algorithm by immersion [22]. The TNTs were detected using the method in [23], except from the edge detection, which was replaced by adaptive thresholding [21]. Every detected cell was labeled as either CTB positive, DiD positive or neutral, in the following referred to as 'CTB' cells, 'DiD' cells or 'unstained' cells, respectively. The labeling of the cells was accomplished by converting the CTB and DiD channel into binary images by thresholding. For the CTB channel, a global thresholding was suitable since the images are homogenous, but the DiD channel required an adaptive thresholding for the binarization due to the varying signal intensity. Both thresholding techniques convert the respective channels into binary images with pixel values '1' and '0'. A cell was classified as CTB or DiD positive, if it had at least $4/3\pi r^3$ associated '1'-pixels in the respective channels, where r is the smallest allowed radius of an organelle, which was estimated to 153 nm. A cell positive for both CTB and DiD was said to be double positive and those cells were of special interest since DiD organelles have obviously been transferred.

We defined four groups of cells, A, B, C and D, shown in Fig. 5A: (A) double positive cells with a TNT to a DiD cell, (B) acceptor cells with a TNT to a DiD cell, (C) double positive cells without a TNT to a DiD cell and (D) acceptor cells without a TNT to a DiD cell. From these definitions it follows that $A \subseteq B$ and $C \subseteq D$ since every double positive cell is also an acceptor cell. Furthermore, let $\{A \cup B \cup C \cup D\} \cap G = \varnothing$ where G is the set of acceptor cells with at least one direct donor neighbor. Thus, these cells were excluded from the analysis to minimize the influence of neighbor cells.

The TNT number was counted and directly compared between the 24-h control and 24-h CytoB condition. The overall transfer in the 24-h time point in the presence of CytoB was normalized by subtracting the transfer in the 2-h time point. Let $n(x,y)$ be the *number of cells* in group x at time point y and define the transfer rate at time point y as $tr(y) = (n(A,y) + n(C,y))/(n(B,y) + n(D,y))$. Then, the transfer rate TR between the time points was computed as $TR = (tr(24\text{ h}) - tr(2\text{ h})) * 100\%$. The correlation between TNT connected cells and transfer was also computed. This analysis was performed by comparing group A/B to group C/D after subtracting the transfer rate $tr(24\text{ h})$ (Fig. 5B). This normalization

was necessary due to variation of transfer between the experiments. Thus, the statistics was computed from comparing $n(A,24\text{ h})/n(B,24\text{ h}) - tr(24\text{ h})$ with $n(C,24\text{ h})/n(D,24\text{ h}) - tr(24\text{ h})$, and similarly for the 2 h condition.

3. Results

3.1. Analysis of formation and lifetime of TNTs

To investigate the formation of TNTs between PC12 cells, we performed high-resolution DIC microscopy. A statistical analysis of 100 events of formation revealed that 93% of TNTs arose from filopodial interplay near the substrate, followed by filopodial retraction and generation of TNTs (Fig. 1A). The remaining 7% TNTs were generated after dislodgment of cells (Fig. 1B). Furthermore, the lifetime of TNTs ($n = 107$), i.e. the time span between their formation and their fracture, was determined from the acquired movies. The obtained data are depicted in a frequency plot (Fig. 1C). The majority of the TNTs had short lifetimes and only a few percent lasted for longer than 1 h. This is reflected by a median value of 7 min (Fig. 1C, arrow) and demonstrates the transient nature of TNTs in PC12 cells.

3.2. Effect of CytoB on formation and stability of TNTs

Because 93% TNTs form by filopodial interplay of PC12 cells, we investigated whether interference with the formation of filopodia would result in a reduction of TNTs. First, we tested the efficiency of CytoB to eliminate filopodia from PC12 cells. Three different concentrations of CytoB (175 nM, 350 nM and 700 nM) were used and the effects were analyzed by DIC microscopy. Whereas 175 nM CytoB had a weak effect, the 700 nM had a similar effect as the 350 nM (data not shown). To minimize side effects on the cells, we chose a concentration of 350 nM CytoB for the subsequent

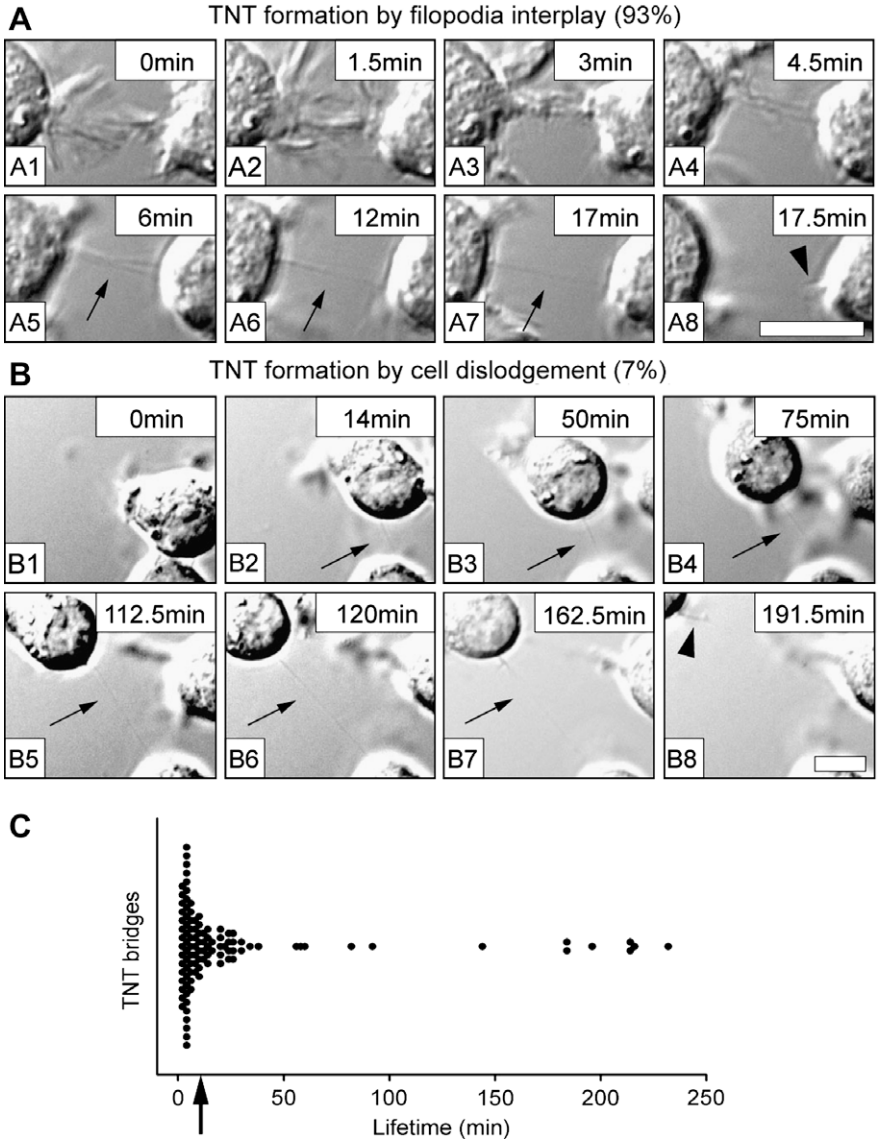

Fig. 1. Formation and lifetime of tunneling nanotubes (TNTs) in PC12 cell cultures. (A) TNT formation by filopodial interplay was observed in 93% of the analyzed structures. Firstly, filopodia interact near the substratum (A1–A3), followed by filopodial retraction (A4) and subsequent formation of a TNT (A5). The TNT persists for 11.5 min, indicated by the arrows in (A5–A7). Remnants of the TNT after breakage are indicated by the arrowhead in (A8). (B) TNT formation by cell dislodgement was observed in 7% of the analyzed structures. Adjacent cells dislocate slowly from each other (B1–B2). After 14 min a TNT becomes visible, and remains stable for 177.5 min, indicated by the arrows (B2–B7). Remnants of the TNT after breakage are indicated by the arrowhead in (B8). (C) Frequency plot displaying the lifetime of TNTs between PC12 cells. The lifetime of TNTs ($n = 107$) was analyzed by DIC microscopy. The arrowhead indicates the median lifetime of 7 min. Scale bars, 5 μm.

experiments. This led to a disappearance of all filopodia within 390 ± 42 s (n = 7 movies).

We then addressed whether drug treatment reduced the number of TNT structures. PC12 cells were cultured in the presence of 350 nM CytoB and subjected to 3D fluorescence microscopy. The analysis of optical sections from the middle of the cells, where TNTs are typically located, revealed that the number of TNTs was strongly reduced after 6 h of CytoB treatment (compare Fig. 2A1 and A3). At the same time, cell protrusions attached to the substratum showed the efficient elimination of filopodial structures, whereas lamellipodial sheets were unaffected under these conditions (compare Fig. 2A2 and A4).

To analyse the time effect of CytoB on the number of TNTs, image stacks were acquired after different time points of drug application and subjected to automatic analysis of TNT frequency [23]. Interestingly, this showed a fast and strong decrease of TNTs upon CytoB treatment by 80% after 30 min of 350 nM CytoB incubation as compared to control conditions (Fig. 2B). To further investigate whether this strong reduction was due to a block of TNT formation or to rupture of existing TNTs, we performed two types of experiments. First, we quantitatively monitored the formation of new TNTs during the first hour of drug treatment by employing confocal time-lapse microscopy. Under control conditions, 62 TNTs were present at the start of the imaging and during the first hour 46 new TNTs formed (n = 12 movies). This corresponded to 80% newly formed TNTs. In contrast, in the presence of 350 nM CytoB, 86 TNTs were present at the time point of drug application and only 8 new TNTs formed during the first hour of

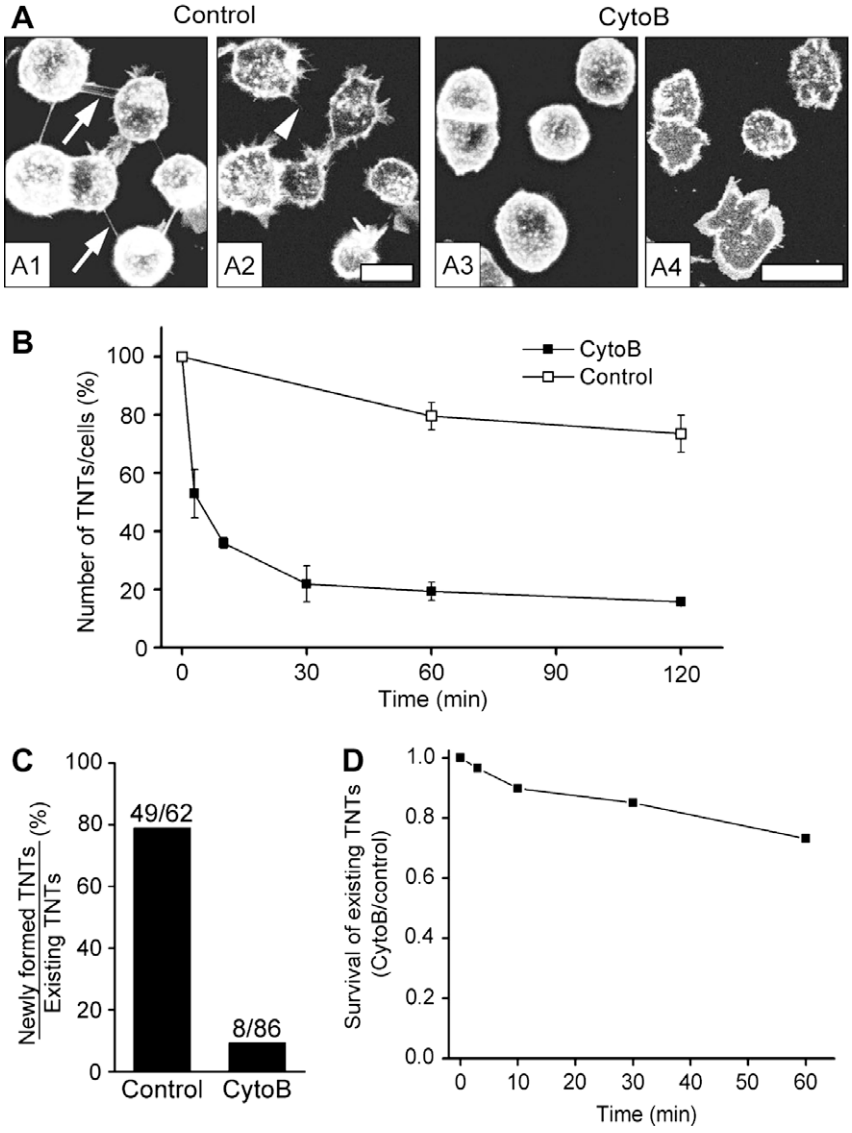

Fig. 2. Low concentration of CytoB inhibits filopodia formation and reduces the number of TNTs. (A) PC12 cells were incubated for 6 h with or without 350 nM CytoB, stained with WGA488 directly before imaging and recorded in 3D by confocal microscopy. Shown are maximum intensity projections of the upper focal planes of a representative image stack from control (A1) and drug-treated (A3) cells. Arrows indicate TNTs. Note the absence of TNT connectivity in the drug-treated cells as compared to control condition. (A2) and (A4) depict single focal planes near the substratum of the image stacks shown in (A1) and (A3), respectively. Filopodia, frequently visible in untreated cells (A2, arrowhead), are absent after drug treatment (A4). (B) TNT number decreases in the presence of CytoB. PC12 cells were incubated with 350 nM CytoB for different times, and analyzed for TNT numbers by wide-field fluorescence imaging combined with automated cell segmentation and TNT detection (see also Fig. 3A). For each time point 1500–2000 cells from at least three independent experiments were analyzed. (C) CytoB blocks the formation of new TNTs. WGA488 stained PC12 cells were incubated with 350 nM CytoB and subjected to time-lapse fluorescence imaging using the resonant scanner of the confocal microscope. From the obtained 3D stacks the number of existing TNTs at the timepoint of CytoB addition and the newly formed TNTs during the first hour of incubation were counted. The graph shows the ratio of newly formed TNTs to existing TNTs in percent. (D) CytoB has a weak effect on TNT stability. The survival of existing TNTs was determined from the respective 3D stacks of (C) at the different time points. The graph shows the ratio of TNT number in the presence (n = 119 TNTs) and absence (n = 62 TNTs) of 350 nM CytoB.

drug incubation ($n = 17$ movies). This corresponded to only 10% newly formed TNTs (Fig. 2C). Second, we statistically analyzed how long existing TNTs monitored at time zero remained in the presence of 350 nM CytoB or under control conditions. The obtained survival of existing TNTs was expressed as the ratio of remaining TNTs in the presence versus absence of the drug (Fig. 2D). This ratio decreased by about −15% TNTs during 30 min, indicating that CytoB had only a weak effect on the stability of TNTs.

Thus, incubation of PC12 cells with 350 nM CytoB interferes with the formation of TNTs but hardly affects their stability after formation.

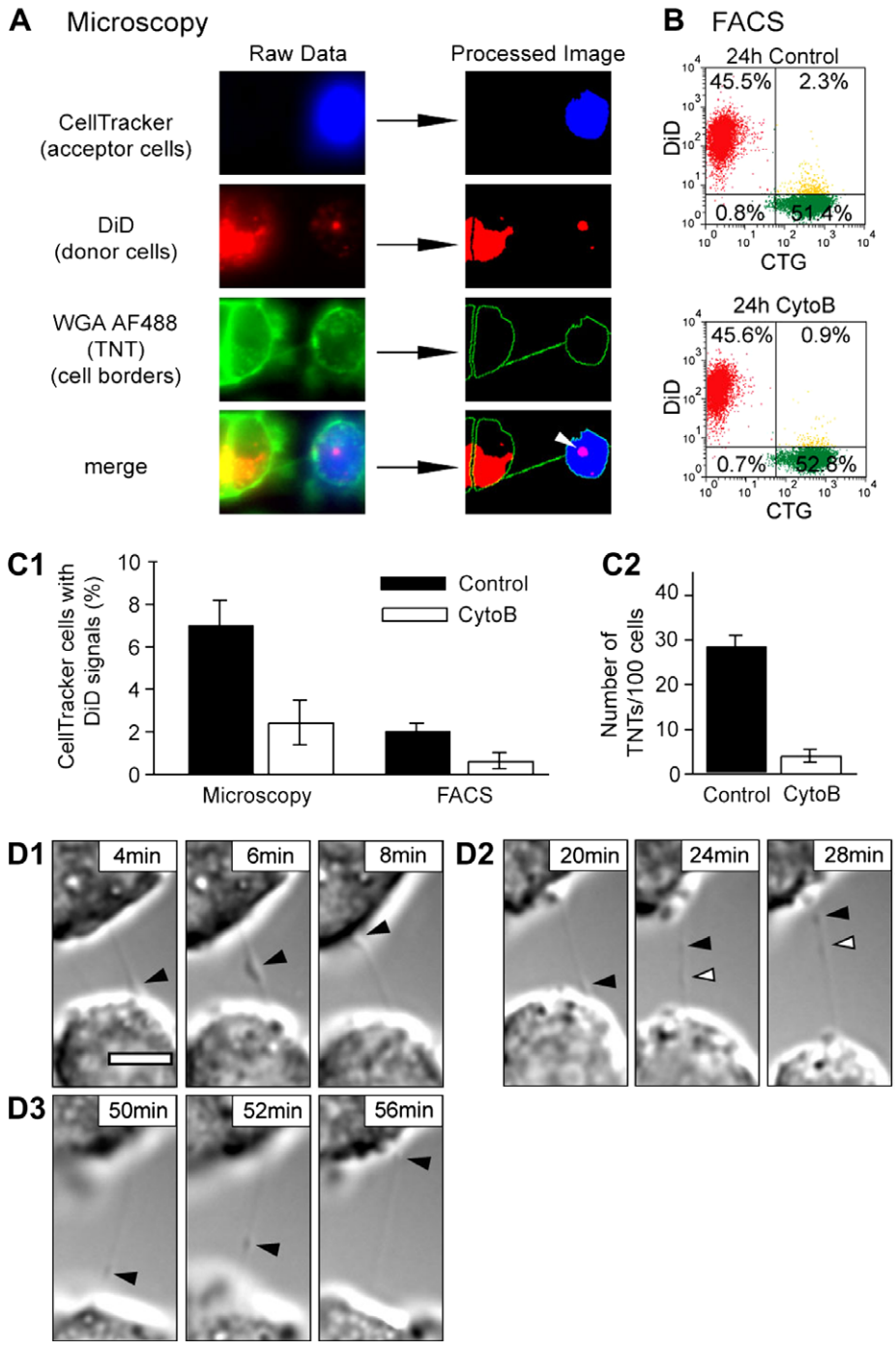

Fig. 3. Low concentration of CytoB reduces intercellular organelle transfer. (A) Cocultures of DiD (donor) and CellTracker (acceptor) PC12 cell populations were analyzed by microscopy or FACS for organelle transfer. Illustration of automated and quantitative image analysis of microscopy data to study organelle transfer. Shown are the raw (left) and processed images (right) of the three channels recorded as well as their merge (lowest panel). The WGA488 channel is used both for a global cell segmentation and for TNT detection as described in [23]. The acquired DiD signals in the TNT connected CTB-stained cell is marked with an arrowhead. (B) Dot plot diagrams depicting organelle transfer analyzed by FACS. Donor populations (DiD-stained cells) are shown in red in the upper left quadrant, acceptor populations (CTG-stained cells) are shown in green in the lower right quadrant. CTG cells exhibiting transfer of DiD are depicted in yellow in the upper right quadrant. (C) Treatment of cells with 350 nM CytoB revealed a reduction in both organelle transfer (C1) and TNT numbers (C2) after 24 h. For microscopic analysis of organelle transfer, in total ~18 000 cells were analyzed. At least four independent experiments were carried out for each condition. The TNT number was determined by automated cell segmentation and TNT detection. (D) CytoB does not block the transfer activity of TNTs. PC12 cells were monitored by time-lapse DIC microscopy during the first hour after addition of 350 nM CytoB. Vesicle-like structures (marked with arrowheads) move from one cell to another along the TNT at indicated timepoints: 4 min (D1), 20 min (D2) and 50 min (D3), respectively. Scale bar, 5 μm.

3.3. Effect of CytoB on organelle transfer

Prompted by our results showing a specific inhibition of TNT formation by CytoB, we addressed if this drug also affects the TNT-dependent organelle transfer. To obtain measurable values for organelle transfer, a 24 h incubation time was chosen. To monitor endocytic organelle transfer, we established a robust coculturing system consisting of organelle donor and acceptor cell populations. Organelle donor populations were labeled with red fluorescent DiD. As an acceptor population, cells were labeled either with CTB or CTG for microscopy or FACS analysis, respectively (Fig. 3A and B). The cocultures were analyzed after 2 and 24 h of incubation. Previous studies had shown that TNT formation between PC12 cells started after proper cell attachment and the number of TNTs reached a plateau 3 h after plating. Therefore, the transfer rate after 2 h was considered as unspecific background and was subtracted from the 24 h transfer value. Automated image processing of microscopic data showed that organelle transfer rates under control and CytoB conditions over 24 h were 7.0 ± 1.1% (±S.E.M.) and 2.4 ± 1.1% (±S.E.M.), respectively (Fig. 3C1). Cocultures analyzed by FACS displayed transfer rates of 2.0 ± 0.3% (±S.E.M.) and 0.6 ± 0.4% (±S.E.M.), respectively (Fig. 3C1). This indicates a ~3-fold decrease in organelle transfer. Furthermore, microscopic analysis of the TNT number from the obtained image stacks used for the estimation of organelle transfer after 24 h showed a reduction of TNT structures from 28 ± 2.3 (±S.E.M.) per 100 cells under control conditions to 3.9 ± 1.5 (±S.E.M.) in the presence of CytoB (Fig. 3C2). This indicates a 7.2-fold decrease ($P < 0.001$, two-tailed t-test) in TNT number.

Interestingly, during our real time studies we observed that vesicle-like structures were still transferred from one cell to another along a TNT in the presence of 350 nM CytoB (Fig. 3, D1-D3, Supplemental movie 1). These transport events occurred during three time intervals starting at 4 min, 20 min and 50 min after application of CytoB. This may indicate that the TNT-dependent transfer of vesicle-like structures in already existing TNTs is not affected by CytoB treatment.

To obtain further evidence that the reduction in intercellular organelle transfer is caused by a CytoB-induced reduction in TNT number, we studied whether phagocytosis and endocytosis were affected by CytoB treatment. First, we analyzed the uptake of fluorescently labeled cell debris in the presence and absence of CytoB by 3D wide-field microscopy (Fig. 4A1). A statistical investigation of such preparations employing automated image analysis indicated that there was no significant difference in the phagocytotic uptake of cell debris after treatment with CytoB as compared to control conditions (Fig. 4A2). Second, PC12 cells were briefly incubated in WGA633-containing medium in the absence and presence of 350 nM CytoB and the intensities of the endocytosed signals were quantified (Fig. 4B1). After quantitative image analysis, these experiments showed no significant difference in the endocytosis of WGA633 (Fig. 4B2). Taken together, the observed reduction of organelle transfer between PC12 cells in the presence of CytoB cannot be explained by an inhibition of phagocytic or endocytic processes. Rather, in light of our finding that CytoB decreases organelle transfer and TNT number without affecting the TNT-dependent transfer activity, our data suggests that the decline in organelle transfer is caused by a CytoB-induced inhibition of TNT formation.

3.4. Correlation of organelle transfer and TNT connection

By combining the automated protocol to detect TNTs and organelle transfer in cocultures of acceptor and donor cell populations, we were able to perform a thorough analysis of the probability of an acceptor cell receiving an organelle from a donor cell if a TNT

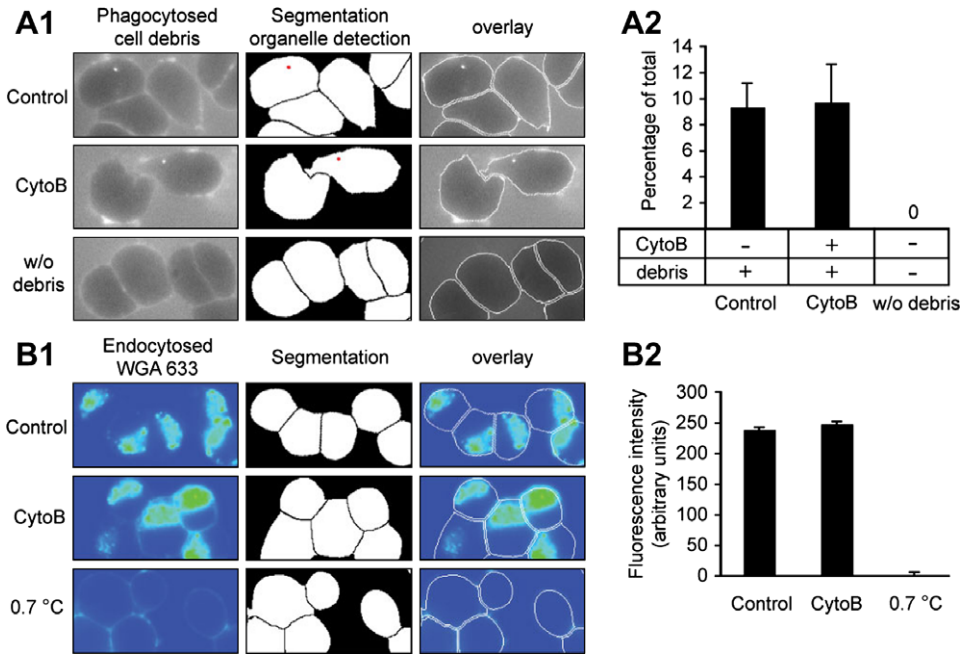

Fig. 4. Low concentration of CytoB has no effect on phagocytosis and fluid-phase endocytosis. PC12 cells were analyzed for phagocytosis of DiI-stained cell debris and for endocytosis of WGA633. (A) CytoB treatment has no effect on phagocytosis. Representative single focal planes of the recorded image stacks for the different conditions are shown as indicated (A1). 9.3 ± 1.1% (±S.E.M.) and 9.7 ± 1.7% (±S.E.M.) of the analyzed cells displayed internalized cell debris signals in control and CytoB treated conditions, respectively (A2). In total, ~3000 cells from at least three independent experiments were analyzed. (B) CytoB treatment has no effect on fluid-phase endocytosis. Representative single focal planes of the recorded image stacks for different conditions analyzing endocytosis of WGA633 are shown as indicated (B1). The bright WGA633 signals inside the cells showed a similar pattern under control and CytoB conditions. In contrast, the sample incubated at 0.7 °C displays only a peripheral plasma membrane staining. Normalized fluorescence intensities (see Section 2.6) of WGA633 inside the segmented cell borders are 238 ± 7.9% (±S.E.M.) and 247 ± 8.1% (±S.E.M.) (B2). Note the insignificant difference between the control and the CytoB-treated samples in A2 and B2, respectively.

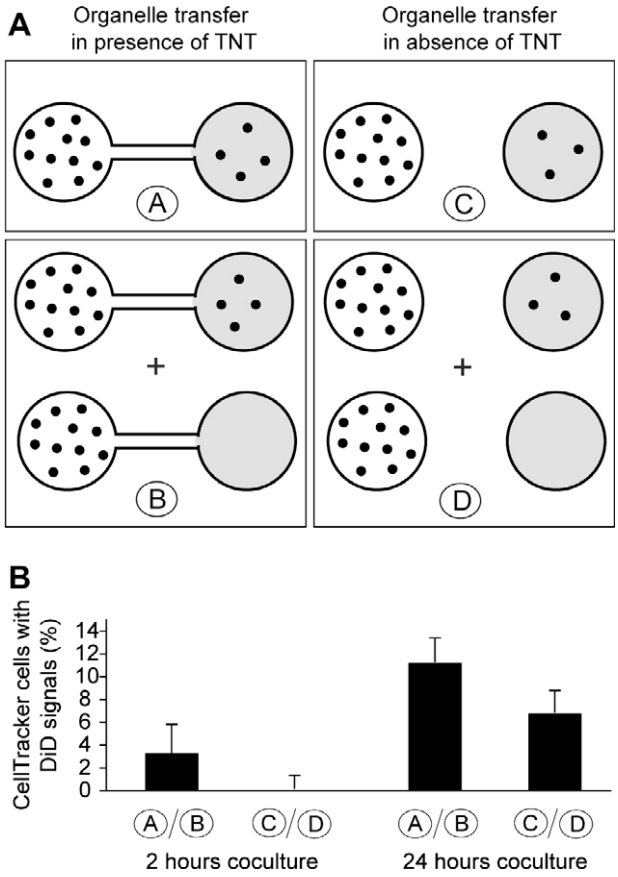

Fig. 5. Correlation of TNT and organelle transfer. Cocultures of DiD and CTG labeled PC12 cells were subjected to imaging 2 and 24 h after plating. The obtained image stacks were analyzed by automated 3D image segmentation (see also Fig. 3A). (A) The segmented CTB-stained cells are classified into four different groups (see Section 2.6) (B) Ratios of the groups A/B (TNT-correlated transfer) and the groups C/D (non-correlated transfer) are displayed for the 2 and 24 h after plating. Note the correlation increased over time. In total ~18 000 cells from 10 independent experiments were analyzed.

was present (Fig. 5, see also Fig. 3A). To do so, we compared the percentage of acceptor cells that exhibited transfer and possessed a TNT connection to donor cells (ratio A/B, correlated transfer, Fig. 5A) to the percentage of acceptor cells that exhibited transfer but did not have a TNT connection to a donor cell (ratio C/D, non-correlated transfer, Fig. 5A) (see also Section 2.6). This showed that 2 h after start of the coculture the correlated transfer of 3.3 ± 2.5% (±S.E.M.) (ratio A/B) was slightly above the non-correlated background (ratio C/D), but this increase was insignificant ($P = 0.08$, two-tailed t-test) (Fig. 5B, 2 h coculture). After 24 h, the TNT-specific transfer increased to 11.2 ± 2.1% (±S.E.M.) (ratio A/B) as compared to 6.8 ± 1.9% (±S.E.M.) for non-correlated transfer (ratio C/D), and this differential increase was very significant ($P = 0.001$, two-tailed t-test) (Fig. 5B, 24 h coculture). It is of note that the probability for a CellTracker-stained cell to possess DiD-stained organelles was 64% higher when it had a TNT to a DiD-stained cell at this time point.

4. Discussion

In this work we report on the specific inhibition of TNT formation between PC12 cells by nanomolar concentrations of CytoB. Given that the majority of TNTs was formed from filopodia in PC12 cells, the removal of filopodia by treatment with 350 nM of CytoB resulted in a strong inhibition of TNT formation. The precise molecular mechanism of the CytoB effect on the inhibition of filopodia outgrowth is unknown. However, several lines of evidence suggest that this F-actin binding toxin might specifically compete with F-actin nucleating proteins such as Ena/VASP at the filopodial tip [16,17,24]. Interestingly, CytoB had only a weak effect on the stability of already formed TNT, implying that F-actin tip nucleators might not be important for the stability of formed TNT. Thus, although TNTs originate from filopodia, they develop into F-actin-based bridges with a unique morphology and distinct properties.

Our study showed that a selective block of TNT formation by treatment of PC12 cells with 350 nM CytoB resulted in a strong inhibition of TNT-dependent organelle transfer. This result was obtained by two independent evaluation methods, microscopy and FACS. It is of note that the difference in absolute transfer values was due to the different sensitivity of the respective detection methods and the thresholds applied. However, the relative reduction in transfer was strikingly similar in both cases, 2.9- and 3.3-fold for microscopy and FACS, respectively. This reduction was less pronounced than the ~7-fold decrease in TNT number obtained under the same experimental conditions. One reason for this discrepancy may be that during the first few hours of CytoB treatment significantly more TNTs remained as compared to the 24 h time point. Hence, intercellular organelle transfer most likely continued through these TNTs and contributes to the obtained value measured at 24 h (Fig. 3C1). Furthermore, in support of a TNT-specific effect of the drug neither phagocytosis nor endocytosis was affected by the CytoB treatment. Thus, our data provide compelling evidence that the reduction in organelle transfer between PC12 cells is the result of the selective inhibition of TNT formation by CytoB.

In agreement with a TNT-dependent organelle transfer, we obtained a significant correlation between a transfer event and a TNT connection. This was achieved by a thorough statistical analysis of ~18 000 cells applying high-throughput image processing of 3D microscopy data. These studies indicated that the degree of correlation increases over time, resulting in a significant degree of correlation 24 h after proper cell attachment. Given the transient nature of TNT bridges the obtained correlation value is most likely an underestimation of the real correlation. In a previous study we reported on a 74% correlation value between organelle transfer and TNT connection in PC12 cells [1]. However, the analysis was carried out under different experimental conditions (e.g. organelle transfer was measured in both directions, fixed cells were used, different staining procedures were applied, etc.), which may explain the different results.

In conclusion, we show here that filopodia are the main precursors of TNTs in PC12 cells and that the removal of filopodia by low concentration of CytoB will strongly inhibit TNT formation and subsequently reduce TNT-dependent organelle exchange. To our knowledge, this study represents the first demonstration that a selective inhibition of TNT connectivity between cells results in a concurrent interference with cell-to-cell communication. Thus, the treatment of cell populations with low concentration of CytoB provides a valuable tool to further elucidate signaling pathways propagating between cells along TNT bridges.

Acknowledgements

The confocal imaging was performed at the Molecular Imaging Center (FUGE, Norwegian Research Council), University of Bergen. The authors are grateful for the generous financial support of the Norwegian Cancer Society (J.F.V.B., E.H., H.-H.G.), the Norwegain Research Council (X.W.), the University of Bergen/Nanoscience Programme, Norway (N.V.B., H.-H.G.) and the Gottlieb Daimler- and Karl Benz-Foundation, Germany (S.G.).

Appendix A. Supplementary material

Supplementary data associated with this article can be found, in the online version, at doi:10.1016/j.febslet.2009.03.065.

References

[1] Rustom, A., Saffrich, R., Markovic, I., Walther, P. and Gerdes, H.H. (2004) Nanotubular highways for intercellular organelle transport. Science 303, 1007–1010.

[2] Gerdes, H.H., Bukoreshtliev, N.V. and Barroso, J.F. (2007) Tunneling nanotubes: a new route for the exchange of components between animal cells. FEBS Lett. 581, 2194–2201.

[3] Davis, D.M. and Sowinski, S. (2008) Membrane nanotubes: dynamic longdistance connections between animal cells. Nat. Rev. Mol. Cell Biol. 9, 431–436.

[4] Gurke, S., Barroso, J.F. and Gerdes, H.H. (2008) The art of cellular communication: tunneling nanotubes bridge the divide. Histochem. Cell Biol. 129, 539–550.

[5] Koyanagi, M., Brandes, R.P., Haendeler, J., Zeiher, A.M. and Dimmeler, S. (2005) Cell-to-cell connection of endothelial progenitor cells with cardiac myocytes by nanotubes: a novel mechanism for cell fate changes? Circ. Res. 96, 1039–1041.

[6] Onfelt, B., Nedvetzki, S., Benninger, R.K., Purbhoo, M.A., Sowinski, S., Hume, A.N., Seabra, M.C., Neil, M.A., French, P.M. and Davis, D.M. (2006) Structurally distinct membrane nanotubes between human macrophages support long-distance vesicular traffic or surfing of bacteria. J. Immunol. 177, 8476–8483.

[7] Onfelt, B., Nedvetzki, S., Yanagi, K. and Davis, D.M. (2004) Cutting edge: Membrane nanotubes connect immune cells. J. Immunol. 173, 1511–1513.

[8] Watkins, S.C. and Salter, R.D. (2005) Functional connectivity between immune cells mediated by tunneling nanotubules. Immunity 23, 309–318.

[9] Sowinski, S., Jolly, C., Berninghausen, O., Purbhoo, M.A., Chauveau, A., Kohler, K., Oddos, S., Eissmann, P., Brodsky, F.M., Hopkins, C., Onfelt, B., Sattentau, Q. and Davis, D.M. (2008) Membrane nanotubes physically connect T cells over long distances presenting a novel route for HIV-1 transmission. Nat. Cell Biol. 10, 211–219.

[10] Eugenin, E.A., Gaskill, P.J. and Berman, J.W. (2009) Tunneling nanotubes (TNT) are induced by HIV-infection of macrophages: a potential mechanism for intercellular HIV trafficking. Cell Immunol. 254, 142–148.

[11] Chinnery, H.R., Pearlman, E. and McMenamin, P.G. (2008) Cutting edge: membrane nanotubes in vivo: a feature of MHC class II+ cells in the mouse cornea. J. Immunol. 180, 5779–5783.

[12] Chhabra, E.S. and Higgs, H.N. (2007) The many faces of actin: matching assembly factors with cellular structures. Nat. Cell. Biol. 9, 1110–1121.

[13] Rottner, K., Behrendt, B., Small, J.V. and Wehland, J. (1999) VASP dynamics during lamellipodia protrusion. Nat. Cell. Biol. 1, 321–322.

[14] Berg, J.S. and Cheney, R.E. (2002) Myosin-X is an unconventional myosin that undergoes intrafilopodial motility. Nat. Cell Biol. 4, 246–250.

[15] Pellegrin, S. and Mellor, H. (2005) The Rho family GTPase Rif induces filopodia through mDia2. Curr. Biol. 15, 129–133.

[16] Zheng, J.Q., Wan, J.J. and Poo, M.M. (1996) Essential role of filopodia in chemotropic turning of nerve growth cone induced by a glutamate gradient. J. Neurosci. 16, 1140–1149.

[17] Burnette, D.T., Schaefer, A.W., Ji, L., Danuser, G. and Forscher, P. (2007) Filopodial actin bundles are not necessary for microtubule advance into the peripheral domain of Aplysia neuronal growth cones. Nat. Cell. Biol. 9, 1360–1369.

[18] Heumann, R., Kachel, V. and Thoenen, H. (1983) Relationship between NGF-mediated volume increase and priming effect in fast and slow reacting clones of PC12 pheochromocytoma cells. Exp. Cell Res. 145, 179–190.

[19] Gurke, S., Barroso, J.F., Hodneland, E., Bukoreshtliev, N.V., Schlicker, O. and Gerdes, H.H. (2008) Tunneling nanotube (TNT)-like structures facilitate a constitutive, actomyosin-dependent exchange of endocytic organelles between normal rat kidney cells. Exp. Cell Res. 314, 3669–3683.

[20] Harata, N.C., Choi, S., Pyle, J.L., Aravanis, A.M. and Tsien, R.W. (2006) Frequency-dependent kinetics and prevalence of kiss-and-run and reuse at hippocampal synapses studied with novel quenching methods. Neuron 49, 243–256.

[21] Tai, X.C., Hodneland, E., Weickert, J., Bukoreshtliev, N.V., Lundervold, A. and Gerdes, H.H. (2007) Level Set Methods for Watershed Image Segmentation in: (Sgallari, F., Murli, A. and Paragios, N., Eds.), Scale Space and Variational Methods in Computer Vision, Proceedings of the SSVM 07, pp. 178–190, Springer-Verlag Press, Berlin.

[22] Vincent, L. and Soille, P. (1991) Watersheds in Digital Spaces: An Efficient Algorithm Based on Immersion Simulations. IEEE Trans. Pattern Anal. Mach. Intell. 13, 583–598.

[23] Hodneland, E., Lundervold, A., Gurke, S., Tai, X.C., Rustom, A. and Gerdes, H.H. (2006) Automated detection of tunneling nanotubes in 3D images. Cytometry A 69, 961–972.

[24] Lebrand, C., Dent, E.W., Strasser, G.A., Lanier, L.M., Krause, M., Svitkina, T.M., Borisy, G.G. and Gertler, F.B. (2004) Critical role of Ena/VASP proteins for filopodia formation in neurons and in function downstream of netrin-1. Neuron 42, 37–49.